

## Signature of superconductivity in $\text{UBe}_{13}$ as seen by neutron scattering: Superconducting and magnetic energy scales

A. Hiess,<sup>1,2,\*</sup> A. Schneidewind,<sup>3,4</sup> O. Stockert,<sup>5</sup> and Z. Fisk<sup>6</sup>

<sup>1</sup>European Spallation Source ESS AB, P.O. Box 176, SE-22100 Lund, Sweden

<sup>2</sup>Institut Max von Laue, Paul Langevin, 6 rue Jules Horowitz, BP 156, F-38042 Grenoble Cedex 9, France

<sup>3</sup>Jülich Centre for Neutron Science-MLZ, FZ Jülich GmbH, Outstation at MLZ, Lichtenbergstrasse 1, 85747 Garching, Germany

<sup>4</sup>Helmholtz-Zentrum Berlin für Materialien und Energie, Hahn-Meitner-Platz 1, D-14109 Berlin, Germany

<sup>5</sup>Max-Planck-Institut für Chemische Physik fester Stoffe, Nöthnitzer Strasse 40, D-01187 Dresden, Germany

<sup>6</sup>University of California Irvine, 2186 Frederick Reines Hall, Irvine, California 92697, USA

(Received 21 May 2013; revised manuscript received 2 June 2014; published 17 June 2014)

We here present inelastic neutron scattering results on the strongly correlated cubic superconductor  $\text{UBe}_{13}$  ( $T_c = 0.85$  K) obtained on a large single crystal by high-resolution cold neutron three-axis spectroscopy. We observed spin dynamics at a unique momentum space position building up below  $T \sim 50$  K and changing significantly on entering the superconducting state. The observed short-range longitudinal character of the correlations can be understood as a result of competing magnetic interactions. The energy dependence in the normal state reflects the energy scales determined from specific heat, whereas the low-temperature data suggest the opening of a superconducting gap. Our findings are consistent with a superconducting order parameter exhibiting  $s \pm$  or  $d$ -wave symmetry and placing pure  $\text{UBe}_{13}$  in the strong coupling regime.

DOI: [10.1103/PhysRevB.89.235118](https://doi.org/10.1103/PhysRevB.89.235118)

PACS number(s): 75.30.Et, 61.05.F–, 75.10.–b, 77.80.Fm

### I. INTRODUCTION

To investigate the interrelation of magnetism and superconductivity the condensed matter community focuses on materials where both phenomena may not only coexist, but where the spin dynamics may actually stabilize a novel unconventional superconducting state. For several decades this possibility has been actively debated, not only for copper-oxide- and iron-based high- $T_c$  [1] but also for strongly correlated cerium- and uranium-based intermetallic superconductors [2]. Evoked scenarios to understand this interplay include the energy scales in the normal state such as pseudo-gap phases [3], the spin and lattice dynamics reflected in unusual dispersion relations [4], as well as structural properties related to the often layered structures or observed stripe phases [5,6].

The uranium-based superconductor  $\text{UBe}_{13}$  is particularly interesting because of its cubic crystal structure.  $\text{UBe}_{13}$  shows a superconducting transition temperature  $T_c = 0.85$  K in conjunction with a huge electronic coefficient of the specific heat  $\gamma > 1$  J/molK<sup>2</sup>, indicating strong electronic correlations, but no (long-range) magnetic order [7]. The large specific heat anomaly on entering the superconducting state as well as the temperature dependence of the upper critical field leading to  $B_{c2}(0) = 12$  T indicate the renormalized fermions of the normal state condense at  $T_c$ . Thermodynamic measurements and inelastic neutron scattering (INS) experiments have been used to identify the origin of the unusual electronic properties. An observed phonon resonance in the density of states is related to vibrations of the uranium atoms inside its cage of 24 Be atoms but cannot account for the low-temperature electronic properties [8]. An early low-resolution INS experiment [9] on  $\text{UBe}_{13}$  powder samples identified spin dynamics characterized

by a broad response function ( $\Gamma/2 = 13$  meV), which is probably related to the Schottky-like anomalies observed in specific heat above  $T \sim 100$  K and attributed to CEF excited states [10]. The energy scale observed in subsequent powder experiments [11] and rationalized by a narrow quasielastic response function ( $\Gamma/2 = 1.5$  meV) could be the origin for the shallow so-called “Kondo” maximum at about 20 K in the specific heat [10] largely responsible for the observed heavy electron mass. Assuming Fermi-liquid theory [12] this spin dynamics is consistent with the enhanced Sommerfeld coefficient in the normal state exceeding 1 J/molK<sup>2</sup>. On the other hand, and considering the doping dependence in the specific heat data, Kim *et al.* [13] attribute about half of the electronic specific heat to single-ion effects and the remaining to correlation effects. In more recent INS experiments using pure [14] and Th-doped [15]  $\text{UBe}_{13}$  single crystals short-range and short-lived longitudinal antiferromagnetic (AF) fluctuations characterized by a propagation vector  $k_0 = (1/2, 1/2, 0)$  were observed.

A lower energy scale has been reported that manifests itself by weak anomalies at  $T = 2$  K in high-precision heat capacity and thermal expansion measurements on pure  $\text{UBe}_{13}$  single crystals [16–18]. It has been concluded that only about 5% of potential  $\text{U}^{3+}$  magnetic moments contribute to this 2 K anomaly when comparing to the total entropy and assuming a degenerate (possibly singlet to triplet) two-level system [16]. The temperature of this anomaly, e.g., the underlying energy scale decreases on Th-doping and for 3% Th-doping corresponds to the upper boundary of the superconducting phase [17]. For further understanding, it is important to study the electronic properties also at a microscopic scale. We therefore contribute with INS measurements to (i) identify the microscopic origin of this anomaly at 2 K and (ii) investigate the influence of the superconductivity on the spin dynamics as evidenced in several other cerium- and actinide-based unconventional superconductors [19–27].

\*arno.hiess@esss.se

## II. EXPERIMENTAL

All INS experiments were performed on a large  $\text{UBe}_{13}$  single crystal ( $m \sim 2.5$  g,  $V \sim 0.5$  cm<sup>3</sup>) already used in previous experiments [14]. For its characterization we measured the temperature dependence of the AC susceptibility using an experimental setup homemade for such large crystals. In agreement with literature [7] we observe a superconducting transition with a sharp onset at  $T_c = 0.85$  K and bulk superconductivity reached below  $T = 0.7$  K. The INS experiments reported here were carried out on the cold neutron three-axis spectrometers (TAS) IN14 at the Institut Laue, Langevin, Grenoble, France, and PANDA at MLZ Garching, Germany. For the study of the momentum space dependence of the spin fluctuations, the multi-analyzer-detector FlatCone setup [28] was used on IN14 with fixed final energy of  $E_f = 3.9$  meV ( $k_f = 1.4$  Å<sup>-1</sup>). High-resolution INS experiments on IN14 and PANDA used a single-analyzer-detector setup equipped with a focusing PG002 analyzer set to a fixed final energy  $E_f = 2.7$  meV ( $k_f = 1.15$  Å<sup>-1</sup>). This setup provides an energy resolution of  $\Delta E \leq 65$  μeV. For low-temperature investigations we used dilution refrigerators and for measurements in magnetic field a  $B_{\text{max}} = 15$  T split-coil cryomagnet.

## III. RESULTS

### A. Momentum space and temperature dependence of the spin dynamics in the normal state

The spin dynamics within the  $(H, H, L)$  plane in the normal state of  $\text{UBe}_{13}$  (Fig. 1) has been explored at  $T = 1.5$  K with an energy transfer  $\Delta E = 0.6$  meV using the FlatCone setup on IN14. Besides tails of the strong nuclear Bragg peaks, some weak scattering intensity is clearly visible close to positions  $Q_0 = (\pm 1/2, \pm 1/2, 2)$ . Cutting through the data along the  $(H, H, 2)$  direction [Fig. 1 (c)] reveals unambiguously broad peaks at  $Q = (\pm 1/2, \pm 1/2, 2)$  as well as at  $Q = (\pm 3/2, \pm 3/2, 2)$ , but no such signal is visible at  $Q = (\pm 3/2, \pm 3/2, 0)$ . Since neutron scattering probes spin components perpendicular to the momentum transfer only, it can be concluded that AF fluctuations with a propagation vector  $k_0 = (1/2, 1/2, 0)$  polarized along the  $k_0$  direction (therefore called longitudinally) are present in  $\text{UBe}_{13}$ . This finding is consistent with the spin dynamics inferred from the few momentum space directions investigated in previous TAS measurements [14,15].

These short-range correlations ensure AF phase coherence of a few spins only. The observed  $Q$  width (Fig. 1) is isotropic within statistics and corresponds to a correlation length  $\xi \approx 30$  Å at  $\Delta E = 0.6$  meV. This is about two-times larger than deduced at  $\Delta E = 1.5$  meV from previous results [14]. The FlatCone data also indicate areas of low neutron scattering intensity, which could be used as momentum-independent background for analysis. To respect an absolute momentum transfer  $|Q|$  similar to  $Q_0 = (1/2, 1/2, 2)$  (red circle in Fig. 1), we have chosen  $Q_{\text{bckgrd}} = (1, 1, 3/2)$  (white circle in Fig. 1) as background position for the experimental investigations.

The inelastic scattering intensity is significantly higher at  $Q_0$  than at  $Q_{\text{bckgrd}}$  for all temperatures below  $T \leq 50$  K (Fig. 2). Confronting our inelastic response with the molar

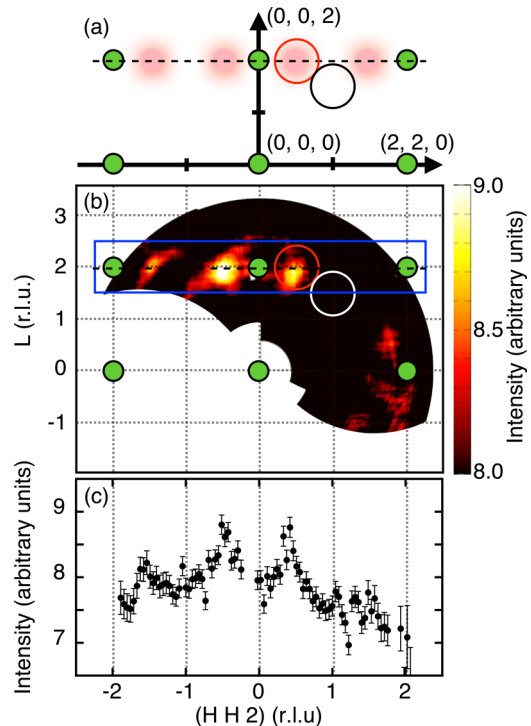


FIG. 1. (Color online) (a) Sketch of the  $(H, H, L)$  scattering plane. Green dots indicate nuclear Bragg peak positions. Fuzzy magenta dots indicate the position of the broad signal observed. The open dot indicates the background position. (b) Intensity map of the normal state dynamic response of  $\text{UBe}_{13}$  in the  $(H, H, L)$  plane at constant energy transfer  $\Delta E = 0.6$  meV and  $T = 1.5$  K using IN14 FlatCone. The observed neutron-scattering intensity is color-coded varying from black (low) to white (high). The red and white circles indicate the momentum space positions  $Q_0 = (1/2, 1/2, 2)$  and  $Q_{\text{bckgrd}} = (1, 1, 3/2)$ , respectively. (c) Cut through the data along the  $(H, H, 2)$  direction with an integration width  $\Delta L = \pm 0.5$  as indicated by the rectangle in the middle panel. The nuclear Bragg peak intensity is outside the scale shown.

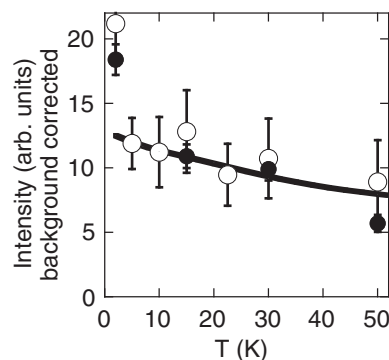


FIG. 2. Temperature dependence of the neutron scattering intensity at  $Q = (1/2, 1/2, 2)$  after subtracting the background contribution at  $Q = (1, 1, 3/2)$ . Integrating the response over energies  $0.15$  meV  $< \Delta E < 1.2$  meV (closed symbols) or averaging single measurements at  $\Delta E = 0.3$  meV and  $\Delta E = 0.6$  meV (open symbols) indicate an accelerated increase of intensity on lowering temperature. Data taken on PANDA with  $k_f = 1.15$  Å<sup>-1</sup>. The solid line shows the temperature dependence of bulk molar susceptibility published by Tou *et al.* [29] (scaled to the units of the plot).

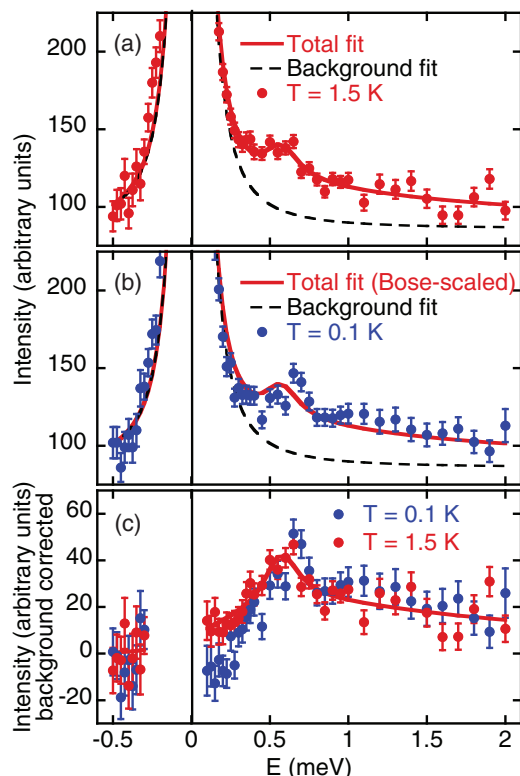


FIG. 3. (Color online) (a) Neutron scattering intensity at  $Q = (1/2, 1/2, 2)$  in the normal state (red dots) of  $\text{UBe}_{13}$  as function of energy transfer. (b) Neutron scattering intensity at  $Q = (1/2, 1/2, 2)$  in the superconducting state (blue dots) of  $\text{UBe}_{13}$  as function of energy transfer. (c) Background corrected neutron scattering intensity at  $Q = (1/2, 1/2, 2)$  in the normal (red dots) and superconducting (blue dots) state of  $\text{UBe}_{13}$  as function of energy transfer. The red line in panels (a) and (c) is a fit of the magnetic signal in the normal state as described in the text. In panel (b), this fit with unchanged parameters has been scaled by the temperature Bose factor to be compared with the data taken in the superconducting state. The dashed black line shows the fit of the temperature-independent intensities at a background position  $Q_{\text{bckgrd}} = (1, 1, 3/2)$ . Data taken on IN14 with  $k_f = 1.15 \text{ \AA}^{-1}$ .

bulk susceptibility from a recent NMR study of Tou *et al.* [29], we find an agreement with their temperature dependence, even if the molar bulk susceptibility and the Knight shift deviate from Curie-Weiss behavior below 35 K. Their conclusion of antiferromagnetic spin fluctuations at a finite  $q$  confirms the magnetic origin of the inelastic scattering results presented here.

On cooling below 2 K, an accelerated increase of magnetic intensity is observed in the neutron data (Fig. 2).

### B. Energy dependence of the spin dynamics

High-resolution INS measurements for energy transfers  $\Delta E \leq 2$  meV were performed to investigate the energy dependence of the spin dynamics at  $Q_0$  in the normal [ $T = 1.5$  K, Fig. 3(a)] and the superconducting state [ $T = 0.1$  K, Fig. 3(b)]. The background corrected data are displayed in Fig. 3(c). In the superconducting state the data appear to be shifted to higher energies. Such a change between the two data sets

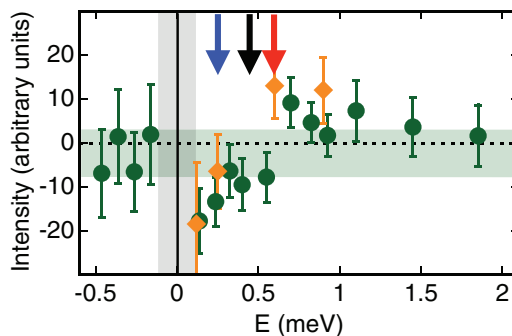


FIG. 4. (Color online) Neutron scattering intensity in the superconducting state subtracted by the neutron scattering intensity in the normal state as a function of energy transfer. Green dots show the  $T$  difference  $I(T = 0.1 \text{ K}) - I(T = 1.5 \text{ K})$  in zero magnetic field. Three or four data points from the raw data presented in Fig. 2 have been binned together and corrected for the Bose temperature factor. Orange diamonds show the magnetic field difference  $I(B = 0 \text{ T}) - I(B = 13 \text{ T})$  at  $T = 0.1$  K. Data taken on IN14. The light green bar indicates the average intensity  $I = -2.5 \pm 5.2$  of all data taken at neutron energy gain (negative energies). Arrows indicate the energy transfer investigated as a function of temperature in Fig. 5.

is further evidenced by subtracting the temperature-corrected data in the normal state from the data in the superconducting state in Fig. 4. For neutron energy loss (negative energies) the intensity  $I = (-2.5 \pm 5.2)$  cts/monitor is close to zero within the error bar as expected and required for data taken at low temperatures. For positive energies  $\Delta E < 0.5$  meV the difference is negative, but a positive difference is observed for  $\Delta E > 0.5$  meV. Intriguingly, the crossover occurs close to the energy at which a pole of the inelastic contribution has been observed in the normal state. To overcome the statistical limitations and exclude potential systematic effects from a single measurement, we further validate our findings by independent measurements. First, to avoid influence from changing the temperature, a magnetic field  $B = 13 \text{ T} > B_{c2}$  was applied to suppress superconductivity at constant temperature  $T = 0.1$  K (orange diamonds in Fig. 4) in a subsequent experiment. The measurements confirm changes in the spin dynamics between normal ( $B = 13 \text{ T}$ ) and superconducting state ( $B = 0 \text{ T}$ ). Second, such a difference is evidenced by the temperature dependence of the spin dynamics at  $Q_0$  and selected energies (colored arrows in Figs. 4 and 5) measured in an independent experiment on another neutron spectrometer. The superconducting transition temperature has been precisely determined by AC susceptibility [Fig. 5(a)] and related to our neutron data. The magnetic response is reduced in the superconducting state at an energy transfer  $\Delta E = 0.25$  meV but augmented at higher energy transfer  $\Delta E = 0.6$  meV with respect to the normal state. All these observations are consistent with a shift of spectral weight from  $\Delta E < 0.6$  meV to  $\Delta E > 0.6$  meV at  $T \approx 0.85$  K, e.g., due to the opening of a superconducting energy gap.

### IV. DATA ANALYSIS

The temperature-independent intensity at  $Q_{\text{bckgrd}}$  exhibits a symmetric line shape in the energy scan centered on

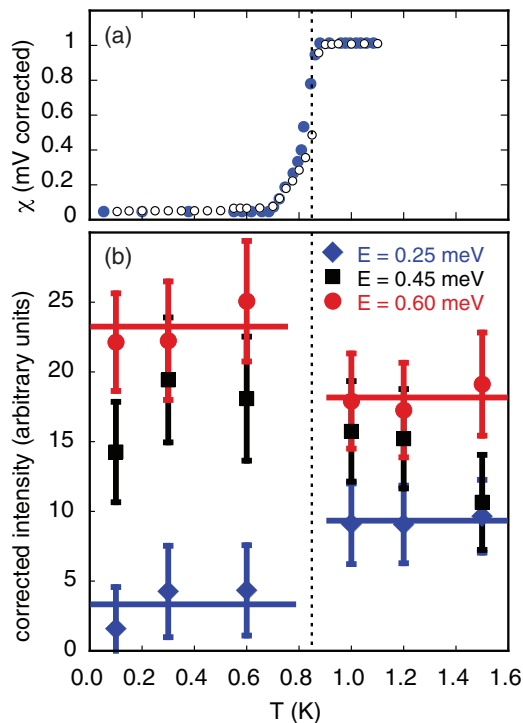


FIG. 5. (Color online) (a)  $T$  dependence of the AC susceptibility measured on the same  $\text{UBe}_{13}$  single crystal used for the INS experiments (open symbols) and compared to literature [10] (closed symbols).  $T_c$  indicated by dotted line. (b)  $T$  dependence of the neutron scattering intensity at  $Q = (1/2, 1/2, 2)$  and different energy transfers. All data are corrected by the Bose temperature factor and for the background contribution at  $Q = (1, 1, 3/2)$ . Data taken on PANDA.

the elastic position. On first glance it seems to reflect a well-behaved (Gaussian) instrumental resolution but closer inspection reveals tails extending symmetrically to  $\Delta E = \pm 0.5$  meV. This line shape is not related to the sample but originates from parasitic (multiple) scattering processes inside materials present along the neutron beam, e.g., the sample environment. Such tails are regularly observed on cold TAS instruments [30]. The line shape can be rationalized using the sum of a constant background level, a narrow Gaussian contribution, and a broad Lorentzian contribution.

Using these phenomenological parameters as background contribution in the analysis of the data taken at  $Q_0$  and  $T = 1.5$  K [Fig. 3 (a)], the additional intensity cannot be fitted with an additional quasielastic contribution only, but requires an inelastic contribution centered at  $\Delta E = 0.55$  meV. This inelastic contribution was fitted with a Gaussian function superimposed to a quasielastic Lorentzian contribution with a characteristic width of 1.5 meV. A single but broad *inelastic* Lorentzian contribution centered at the similar position gives similar statistical errors.

In Fig. 3(b) we confront our low-temperature data with the fit used for data at  $T = 1.5$  K. All parameters have been kept fixed but both quasielastic and inelastic contributions were adjusted using the temperature Bose factor. In this comparison, the low-temperature data appear to be shifted to higher energies with respect to the normal state fit; e.g., the fit exceeds the low- $T$  data points at low energies but falls systematically below

at higher energies. This is nicely visible in Fig. 3(c) in which the same data and fit has been corrected by the background contribution at  $Q_{\text{bckgrd}}$ . This analysis is consistent with the model-free evidence described above (Sec. III B).

## V. DISCUSSION

### A. Competing magnetic interactions in the rare-earth and actinide- $\text{Be}_{13}$ series

The static magnetic properties of rare-earth and actinide- $\text{Be}_{13}$  series enables us to understand the longitudinal magnetic correlations in  $\text{UBe}_{13}$ . Three aspects have to be considered: First, when the  $f$  electrons are localized a unique large magnetic moment will be observed. A more itinerant behavior is often observed for the light actinides. In this case a spin density wave might develop, which is characterized by an amplitude modulation of the magnetic moments. Second, the magnetocrystalline anisotropy will impose the moment direction in respect to the underlying lattice. Third, the RKKY exchange interaction is responsible for the propagation vector of the magnetic structure. When localized moments but no crystalline anisotropy are present, as in the case of  $\text{GdBe}_{13}$ , a helical magnetic structure with an incommensurate propagation vector  $k = (0, 0, 0.285)$  and the  $\text{Gd}^{3+}$  free-ion magnetic moment is observed [31]; see Fig. 6(a). For the other  $\text{REBe}_{13}$  compounds [32] the magnetic structure is commensurate with a propagation vector  $k = (0, 0, 1/3)$  and an irregular helical structure is observed at low temperatures to satisfy the magnetocrystalline anisotropy best; see Fig. 6(b). Here, the ordered moment is reduced by CEF effects. Also in  $\text{NpBe}_{13}$  a commensurate propagation vector  $k = (0, 0, 1/3)$

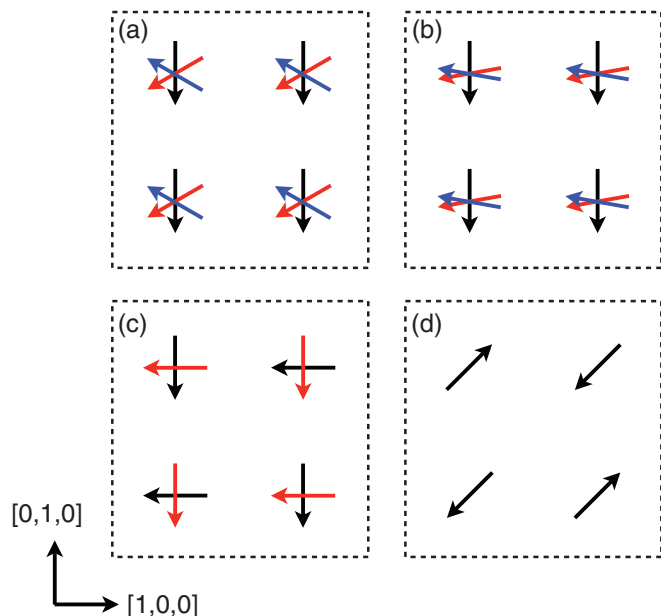


FIG. 6. (Color online) Sketch of the magnetic structure in different rare-earth-based  $\text{REBe}_{13}$  and actinide-based  $\text{ANBe}_{13}$  compounds projected onto the  $(h, k, 0)$  plane. (a) Incommensurate regular helical structure of  $\text{GdBe}_{13}$ , (b) irregular helical structure of other  $\text{REBe}_{13}$  compounds, (c) collinear antiferromagnetic structure of  $\text{NpBe}_{13}$ , and (d) short-range correlations in  $\text{UBe}_{13}$ . Different colors indicate different layers along the propagation axis  $[0, 0, 1]$ .

characterizes the magnetic structure. Nevertheless, in this compound a spin density wave develops on each of the two Bravais lattices [33]. The spins belonging to one spin density wave are collinear but those belonging to different spin density waves are perpendicular to each other; see Fig. 6(c). The resulting unusual spin arrangement breaks the body-centered symmetry but satisfies perfectly the magnetocrystalline anisotropy. The distance between the collinear magnetic moments of each Bravais lattice is larger than for the helical structure with its ferromagnetic spin arrangement in planes perpendicular to the propagation vector. The phases of the two spin density waves are uncorrelated. A spin density wave with two different magnetic moments  $m_1 = 1.0 \mu_B$  and  $m_2 = 1.2 \mu_B$  indicates an itinerant character of the  $5f$  electrons. Finally, as illustrated in Fig. 6(d), the here-discussed short-range spin dynamics of  $\text{UBe}_{13}$  resembles the (orthogonal) in-plane moment arrangement in  $\text{NpBe}_{13}$  considering an average of different magnetic domains. Whereas the RKKY exchange interaction is responsible for magnetic order characterized by a propagation vector  $k \sim (0, 0, 1/3)$  in all other compounds, the small (Kondo-screened) and longitudinally correlated spins do not lead to a magnetically ordered groundstate in  $\text{UBe}_{13}$ .

### B. Spin dynamics in the normal state

Discussing our INS data, Fig. 1 provides evidence that the low-energy spin dynamics is present at a single commensurate momentum space position  $Q_0$  only. In this case,  $Q$  space averaging using powder samples will not alter conclusions on the energy dependence and, indeed, all experimental data from previous [9,11,14] and present INS experiments are consistent with the scenario outlined in the following. The energy dependence of the spin dynamics in the normal state could be modeled phenomenologically superimposing a quasielastic contribution with a Lorentzian line-shape and an inelastic contribution. Both contributions are visible close to  $Q_0$  only, which indicates their common origin. The energy width of the quasielastic contribution ( $\Gamma/2 = 1.5$  meV) observed at  $Q_0$  in  $\text{UBe}_{13}$  is consistent with previous results, whereas the inelastic contribution with a pole at  $\Delta E = 0.55$  meV should lead to a Schottky anomaly  $E \sim 0.42 k_B T_{\max}$  in the specific heat at  $T_{\max} \sim 2.5$  K when employing a two-level model and without considering any momentum space dependence. This matches the energy scale of the weak anomalies observed in high-precision heat capacity and thermal expansion measurements on pure and Th-doped  $\text{UBe}_{13}$  single crystals [16–18]. Moreover, considering the inelastic signal appears sharper in momentum space than the quasielastic contribution, an observed spectral weight of about 10% is quantitatively consistent with the 5% effect deduced from the specific heat data by Kim *et al.* [16] using a two-level localized moment scheme. Also, the accelerated increase in spectral weight on lowering temperatures supports this description.

### C. Spin dynamics in the superconducting state

The link between spin dynamics and (unconventional) superconductivity is often illustrated by a so-called Moriya diagram [34] relating the superconducting transition temperature with the energy scale of the spin dynamics. Indeed,  $\text{UBe}_{13}$  with

$T_c = 0.85$  K, a Sommerfeld coefficient  $\gamma > 1$  J/molK<sup>2</sup> and spin dynamics of a few meV is consistent with this scenario. Our momentum space resolved data taken below  $T_c$  from INS experiments contain significantly more information, especially at low energies. By either confronting the low-temperature data with the fit used at higher temperatures or subtracting both data sets reveals that spectral weight is taken away at low energies  $\Delta E < 0.5$  meV but added at higher energies when the sample is superconducting (Fig. 4). Following the fitting presented above, the data at lowest energies follow strictly the background, i.e., all quasielastic scattering is suppressed below  $T_c$ , whereas the inelastic component is enhanced. For this reason the magnetic signal appears sharper in the superconducting state. In  $\text{UBe}_{13}$  the energy of the additional intensity in the superconducting state and the initial inelastic contribution seems to coincide at a spin gap value of  $\Delta E \sim (0.5 \pm 0.1)$  meV. A large spin gap  $\Delta E \gg k_B T_c$  places pure  $\text{UBe}_{13}$  in the strong coupling regime; see Inosov *et al.* [36] for an overview. Within the scenario of Manske, Eremin, and Bennemann [35], pure  $\text{UBe}_{13}$  resides in the underdoped region of the phase diagram. In other words, the pair breaking mimics the local (singlet to triplet) excitation present already in the normal state. The observed shift of magnetic spectral weight at  $T_c$  (often called “resonance”) by neutron scattering refutes the (early) suggested  $p$ -wave ABM-state [37] and asks for sign-changing  $s\pm$ - or  $d$ -wave superconductivity as suggested by measurements of the Ginzburg-Landau-parameter, untrasonic velocities, and NMR [38]. Also the gap value is compatible with  $s\pm$ - or  $d$ -wave superconductivity.

### D. Comparison with other superconductors

With respect in other superconductors not only the cubic, nonlayered structure in  $\text{UBe}_{13}$  is unusual, but also the observed commensurate short-range correlations. Looking on the heavy-fermion systems, only the spin dynamics of the superconductors  $\text{CeCoIn}_5$  [26] and  $\text{UPt}_3$  [39] have been reported to be short-range at commensurate  $Q$  positions, while in the cubic  $\text{CeIn}_3$  commensurate long-range order is observed before superconductivity occurs under pressure [40] in the vicinity quantum criticality. In all other cases spin dynamics is either observed at incommensurate positions like in  $\text{CeCu}_2\text{Si}_2$  [27] or superconductivity coexists with an AF-ordered state as for the uranium-based superconductors  $\text{UPd}_2\text{Al}_3$  [19–25] and  $\text{UNi}_2\text{Al}_3$  [41]. Also, the magnetic correlations in the iron- and copper-oxide-based superconductors are incommensurate. The energy dependence of the normal state spin dynamics in  $\text{UBe}_{13}$  resembles closely the two-component behavior of the magnetic superconductor  $\text{UPd}_2\text{Al}_3$  [19–25] and  $\text{CeIn}_3$  [42] for which the spin dynamics in the normal state has been described by a fluctuating and an inelastic (spinwave-like) component. In  $\text{UPd}_2\text{Al}_3$ ,  $\text{CeCoIn}_5$ , and  $\text{CeCu}_2\text{Si}_2$  the resonance develops below  $T_c$  similar to observations for optimum- and over-doped copper-oxide-based materials. As evidenced for  $\text{UPd}_2\text{Al}_3$  by high-resolution NSE experiments [43], all quasielastic states at  $Q_0$  below this sharp feature are suppressed in the superconducting state as in  $\text{UBe}_{13}$ . In all compounds the spin dynamics at higher energies beyond this sharp feature remains (almost) unchanged in respect to the normal state. Looking for systematic behavior, heavy-fermion superconductivity is

distinguished neither by layered structures nor by the character of magnetic correlations, only the vicinity to quantum criticality unifies the different systems. However, an intriguing similarity between the phase diagrams is noted for Th-doping [17] of  $\text{UBe}_{13}$ , Ge-doping [44] of  $\text{CeCu}_2\text{Si}_2$  (on a normalized pressure scale), pressure-application [40] on  $\text{CeIn}_3$  and O-doping [5] of the copper-based, Co-doping [5] or (K,Ni)-doping [45] of the iron-based high- $T_c$  superconductors: When the AF-ordered phase is suppressed by some tuning parameter, the low-temperature magnetic (quantum) phase transition is replaced by a superconducting dome. The characteristic transition temperatures meet at the maximum of the superconducting dome.

Our observations in  $\text{UBe}_{13}$  as well as the phase diagram on Th-doping [17] resembles the situation in underdoped copper-based superconductors [46]. In those, an energy scale (“pseudogap” anomaly) is present already in the normal state above  $T_c$ . Similarly, a shift of spectral weight from lower to higher energies appears already in the normal state below the “pseudogap” temperature  $T^*$ . On cooling into the superconducting state this inelastic intensity at higher energies is further enhanced.

Furthermore, not only within a simplistic BCS-like picture as employed for  $\text{UBe}_{13}$ , but shown in more detail for the copper-based high- $T_c$  superconductors [47], the low-energy spin dynamics acts pair-breaking but the higher-energy part of the spectrum is advantageous for superconductivity.

## VI. CONCLUSION

We conclude that unusual longitudinally polarized spin dynamics in  $\text{UBe}_{13}$  builds up on cooling for temperatures below  $T \sim 50$  K at a unique  $Q_0$  position as a result of the competition between moment localization, exchange interactions, and magnetocrystalline anisotropy. The normal state spin dynamics reflects the energy scales observed in heat capacity measurements and determine the superconducting energy scales, i.e.,  $T_c$ . The spin dynamics of  $\text{UBe}_{13}$  at  $Q_0$  changes on entering the superconducting state impacting significantly the lowest normal-state energy scale previously identified at 2.5 K in thermodynamic measurements. The observed shift of spectral weight asks for a sign-changing symmetry of the superconducting order parameter. This observation in a cubic compound could be important to understand unconventional superconductivity.

## ACKNOWLEDGMENTS

The authors acknowledge technical support from ILL and FRM2 for these neutron scattering experiments performed at low temperatures and high magnetic field. We would like to thank D. Argyriou, I. Eremin, B. Fåk, M. M. Koza, G. H. Lander, and F. Steglich for many fruitful discussions.

- 
- [1] P. Monthoux, D. Pines, and G. G. Lonzarich, *Nature* **450**, 1177 (2007).
  - [2] C. Pfleiderer, *Rev. Mod. Phys.* **81**, 1551 (2009).
  - [3] V. Hinkov, P. Bourges, S. Pailhes, Y. Sidis, A. Ivanov, C. D. Frost, T. G. Perring, C. T. Lin, D. P. Chen, and B. Keimer, *Nature Phys.* **3**, 780 (2007).
  - [4] S. Li, C. Zhang, M. Wang, H.-q. Luo, X. Lu, E. Faulhaber, A. Schneidewind, P. Link, J. Hu, T. Xiang, and P. Dai, *Phys. Rev. Lett.* **105**, 157002 (2010).
  - [5] D. J. Scalapino, *Rev. Mod. Phys.* **84**, 1383 (2012).
  - [6] R. Hott, R. Kleiner, T. Wolf, and G. Zwirgagl, in *Handbook of Applied Superconductivity*, edited by P. Seidel (Wiley-VCH, Berlin, in press) [arXiv:1306.0429].
  - [7] H. R. Ott, H. Rudigier, Z. Fisk, and J. L. Smith, *Phys. Rev. Lett.* **50**, 1595 (1983).
  - [8] B. Renker, F. Gompf, J. B. Suck, H. Rietschel, and P. Frings, *Physica B* **136**, 376 (1986).
  - [9] A. I. Goldman, S. M. Shapiro, G. Shirane, J. L. Smith, and Z. Fisk, *Phys. Rev. B* **33**, 1627 (1986).
  - [10] R. Felten, F. Steglich, G. Weber, H. Rietschel, F. Gompf, B. Renker, and J. Beuers, *Europhys. Lett.* **2**, 323 (1986).
  - [11] G. H. Lander, S. M. Shapiro, C. Vettier, and A. J. Dianoux, *Phys. Rev. B* **46**, 5387 (1992).
  - [12] S. M. Hayden, R. Doubble, G. Aeppli, T. G. Perring, and E. Fawcett, *Phys. Rev. Lett.* **84**, 999 (2000).
  - [13] J. S. Kim, B. Andraka, C. S. See, S. B. Roy, and G. R. Stewart, *Phys. Rev. B* **41**, 11073 (1990).
  - [14] S. Coad, A. Hiess, D. F. McMorrow, G. H. Lander, G. Aeppli, Z. Fisk, G. R. Stewart, S. M. Hayden, and H. A. Mook, *Physica B* **276-278**, 764 (2000).
  - [15] A. Hiess, R. H. Heffner, J. E. Sonier, G. H. Lander, J. L. Smith, and J. C. Cooley, *Phys. Rev. B* **66**, 064531 (2002).
  - [16] J. S. Kim and G. R. Stewart, *Phys. Rev. B* **51**, 16190 (1995).
  - [17] M. Lang, R. Helfrich, F. Kromer, C. Langhammer, F. Steglich, G. R. Stewart, and J. S. Kim, *Physica B* **259-261**, 608 (1999).
  - [18] N. Oeschler, F. Kromer, T. Tayama, K. Tenya, P. Gegenwart, G. Sporn, and F. Steglich, *Acta Phys. Pol. B* **34**, 255 (2003).
  - [19] N. Metoki, Y. Haga, Y. Koike, and Y. Onuki, *Phys. Rev. Lett.* **80**, 5417 (1998).
  - [20] N. Bernhoeft, N. Sato, B. Roessli, N. Aso, A. Hiess, G. H. Lander, Y. Endoh, and T. Komatsubara, *Phys. Rev. Lett.* **81**, 4244 (1998).
  - [21] N. K. Sato, N. Aso, K. Miyake, R. Shiina, P. Thalmeier, G. Varelogiannis, C. Geibel, F. Steglich, P. Fulde, and T. Komatsubara, *Nature* **410**, 340 (2001).
  - [22] A. Hiess, N. Bernhoeft, N. Metoki, G. H. Lander, B. Roessli, N. K. Sato, N. Aso, Y. Haga, Y. Koike, T. Komatsubara, and Y. Onuki, *J. Phys: Cond. Matt.* **18**, R437 (2006).
  - [23] N. Bernhoeft, A. Hiess, N. Metoki, G. H. Lander, and B. Roessli, *J. Phys: Cond. Matt.* **18**, 5961 (2006).
  - [24] E. Blackburn, A. Hiess, N. Bernhoeft, and G. H. Lander, *Phys. Rev. B* **74**, 024406 (2006).
  - [25] A. Hiess, E. Blackburn, N. Bernhoeft, and G. H. Lander, *Phys. Rev. B* **76**, 132405 (2007).
  - [26] C. Stock, C. Broholm, J. Hudis, H. J. Kang, and C. Petrovic, *Phys. Rev. Lett.* **100**, 087001 (2008).

- [27] O. Stockert, J. Arndt, E. Faulhaber, C. Geibel, H. S. Jeevan, S. Kirchner, M. Loewenhaupt, K. Schmalzl, W. Schmidt, Q. Si, and F. Steglich, *Nature Phys.* **7**, 119 (2011).
- [28] M. Kempa, B. Janousova, J. Saroun, P. Flores, M. Boehm, F. Demel, and J. Kulda, *Physica B* **385-386**, 1080 (2006).
- [29] H. Tou, K. Morita, H. Kotegawa, N. Tsugawa, M. Sera, Y. Haga, E. Yamamoto, and Y. Onuki, *J. Phys. Soc. Jpn.* **81**, SB024 (2012).
- [30] O. Stockert, M. Enderle, and H. v. Löhneisen, *Phys. Rev. Lett.* **99**, 237203 (2007).
- [31] F. Vigneron, M. Bonnet, A. Herr, and J. Schwiezer, *J. Phys. F: Met. Phys.* **12**, 223 (1982).
- [32] P. Dervenagas, P. Burllet, M. Bonnet, F. Bourdarot, A. Hiess, S. L. Bud'ko, P. C. Canfield, G. H. Lander, J. S. Kim, and G. R. Stewart, *Phys. Rev. B* **61**, 405 (2000), and references therein.
- [33] A. Hiess, M. Bonnet, P. Burllet, E. Ressouche, J. P. Sanchez, J. C. Waerenborgh, S. Zwirner, F. Wastin, J. Rebizant, G. H. Lander, and J. L. Smith, *Phys. Rev. Lett.* **77**, 3917 (1996).
- [34] T. Moriya and K. Ueda, *Rep. Prog. Phys.* **66**, 1299 (2003).
- [35] D. Manske, I. Eremin, and K. H. Bennemann, *Phys. Rev. B* **63**, 054517 (2001).
- [36] D. S. Inosov, J. T. Park, A. Charnukha, Yuan Li, A. V. Boris, B. Keimer, and V. Hinkov, *Phys. Rev. B* **83**, 214520 (2011).
- [37] H. R. Ott, H. Rudigier, T. M. Rice, K. Ueda, Z. Fisk, and J. L. Smith, *Phys. Rev. Lett.* **52**, 1915 (1984).
- [38] Y. Shimitsu, Y. Ikeda, T. Wakabayashi, K. Tenya, Y. Haga, H. Hidaka, T. Yanagisawa, and H. Amitsuka, *J. Phys. Soc. Jpn.* **80**, SA100 (2011), and references therein.
- [39] E. D. Isaacs, P. Zschack, C. L. Broholm, C. Burns, G. Aeppli, A. P. Ramirez, T. T. M. Palstra, R. W. Erwin, N. Stucheli, and E. Bucher, *Phys. Rev. Lett.* **75**, 1178 (1995).
- [40] N. D. Mathur, F. M. Grosche, S. R. Julian, I. R. Walker, D. M. Walker, D. M. Freye, R. K. W. Haselwimmer, and G. G. Lonzarich, *Nature* **394**, 39 (1998).
- [41] N. Aso, B. Roessli, N. Bernhoeft, R. Calemczuk, N. K. Sato, Y. Endoh, T. Komatsubara, A. Hiess, G. H. Lander, and H. Kadowaki, *Phys. Rev. B* **61**, R11867 (2000).
- [42] W. Knafo, S. Raymond, B. Fåk, G. Lampertot, P. C. Canfield, and J. Flouquet, *J. Phys.: Cond. Matt.* **15**, 3741 (2003).
- [43] E. Blackburn, A. Hiess, N. Bernhoeft, M. C. Rheinstadter, W. Haussler, and G. H. Lander, *Phys. Rev. Lett.* **97**, 057002 (2006).
- [44] H. Q. Yuan, F. M. Grosche, M. Deppe, C. Geibel, G. Sparn, and F. Steglich, *Science* **302**, 2104 (2003).
- [45] M. Wang, C. Zhang, X. Lu, G. Tan, H. Luo, Y. Song, M. Wang, X. Zhang, E. A. Goremychkin, T. G. Perring, T. A. Maier, Z. Yin, K. Haule, G. Kotliar, and P. Dai, *Nature Commun.* **4**, 2874 (2013).
- [46] H. F. Fong, P. Bourges, Y. Sidis, L. P. Regnault, J. Bossy, A. Ivanov, D. L. Milius, I. A. Aksay, and B. Keimer, *Phys. Rev. B* **61**, 14773 (2000).
- [47] T. Dahm, V. Hinkov, S. V. Borisenko, A. A. Kordyuk, V. B. Zabolotnyy, J. Fink, B. Büchner, D. J. Scalapino, W. Hanke, and B. Keimer, *Nature Phys.* **5**, 217 (2009).